ACS Energy LETTERS

http://pubs.acs.org/journal/aelccp

Solution-Processed Monolithic All-Perovskite Triple-Junction Solar Cells with Efficiency Exceeding 20%

Ke Xiao,[§] Jin Wen,[§] Qiaolei Han, Renxing Lin, Yuan Gao, Shuai Gu, Yipeng Zang, Yuefeng Nie, Jia Zhu, Jun Xu, and Hairen Tan*

Cite This: *ACS Energy Lett.* 2020, 5, 2819−2826

Read Online

ACCESS | Metrics & More | Article Recommendations | Supporting Information

ABSTRACT: **Very high power conversion efficiencies (PCEs) have been demonstrated by multijunction cells made of epitaxial III−V semiconductors; but they are too expensive to manufacture for terrestrial applications. Multijunction solar cells that can be fabricated with cheap and simple solution-processing techniques offer a lower-cost alternative to reach high PCEs. Here we demonstrate the solution processing of efficient all-perovskite triple-junction solar cells using optimal-bandgap perovskites. Monolithic all-perovskite triple-junction cells with an open-circuit voltage of 2.8 V and a fill factor of 81.1% are obtained by developing interconnecting layers that are compatible with the solution processing of perovskite absorbers. The concept and design here represent an important step toward efficient all-perovskite triple-junction solar cells.**

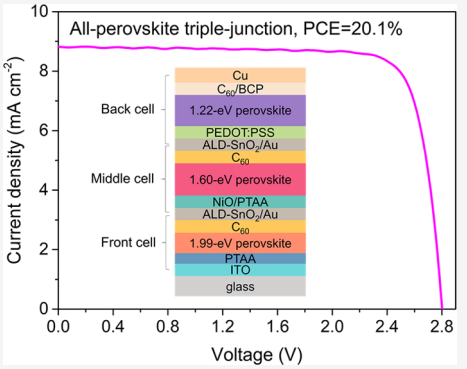

As the photovoltaic (PV) market has increasingly grown, the prices of PV modules have rapidly dropped over the last years.[1] The costs of PV systems are currently dominated by the balance of systems (e.g., installation, cables, and power electronics), which scale with the area of installed PV modules. With advances in manufacture technology and device performance, the mainstream crystalline silicon (c-Si) solar cells are approaching their practical efficiency limit of ∼27%.[2] To further drive down the costs of PV electricity, it is imperative to develop low-cost PV technologies that can largely increase the power conversion efficiencies (PCEs) at the cell and module levels.

Constructing multijunction solar cells with materials having complementary bandgaps offers the promise of raising the PCEs beyond the Shockley−Queisser limit of single-junction solar cells.[3−5] Multijunction solar cells using III−V compound semiconductors have achieved the highest PCEs of 32.8%, 37.9%, and 39.2% under 1-Sun illumination for double-junction (tandem), triple-junction, and six-junction configurations, respectively.[6] Extremely high PCEs up to 47.1% have been attained under concentrated illumination.[7] Solar cells made of III−V semiconductors are, however, too costly to manufacture and deploy for terrestrial applications.[8−10] Utilizing inexpensive materials and processing to fabricate multijunction cells that can attain equivalently high efficiencies is thus of high technological interest for PV research.

Solution-processable metal halide perovskites are becoming attractive for high-efficiency, low-cost multijunction solar cells because of their high optical absorption coefficient,[11] high defect tolerance,[12] simple processing,[13] and tunable bandgaps.[14] The perovskite/c-Si hybrid tandem solar cells have surpassed the highest PCE achieved by c-Si single-junction cells, reaching a certified value of 29.2% by early this year.[15] Perovskite/perovskite/c-Si triple-junction devices are predicted to offer the potential of higher efficiency, though the achieved experimental PCE is only 13.2%.[16]

The bandgaps of perovskites can be continuously tuned between 1.2 and 3.0 eV via compositional engineering, which enables the construction of multijunction solar cells using only perovskite materials.[17,18] Theoretical calculations suggest that the practically achievable PCEs in all-perovskite multijunction cells can go well beyond 30%.[3,19,20] In the past few years, monolithic all-perovskite tandem solar cells have seen a rapid progress in PCEs, mainly because of the advances in developing efficient mixed Pb−Sn narrow-bandgap perovskite

Received: June 1, 2020
Accepted: August 11, 2020
Published: August 11, 2020

https://dx.doi.org/10.1021/acsenergylett.0c01184
ACS Energy Lett. 2020, 5, 2819−2826

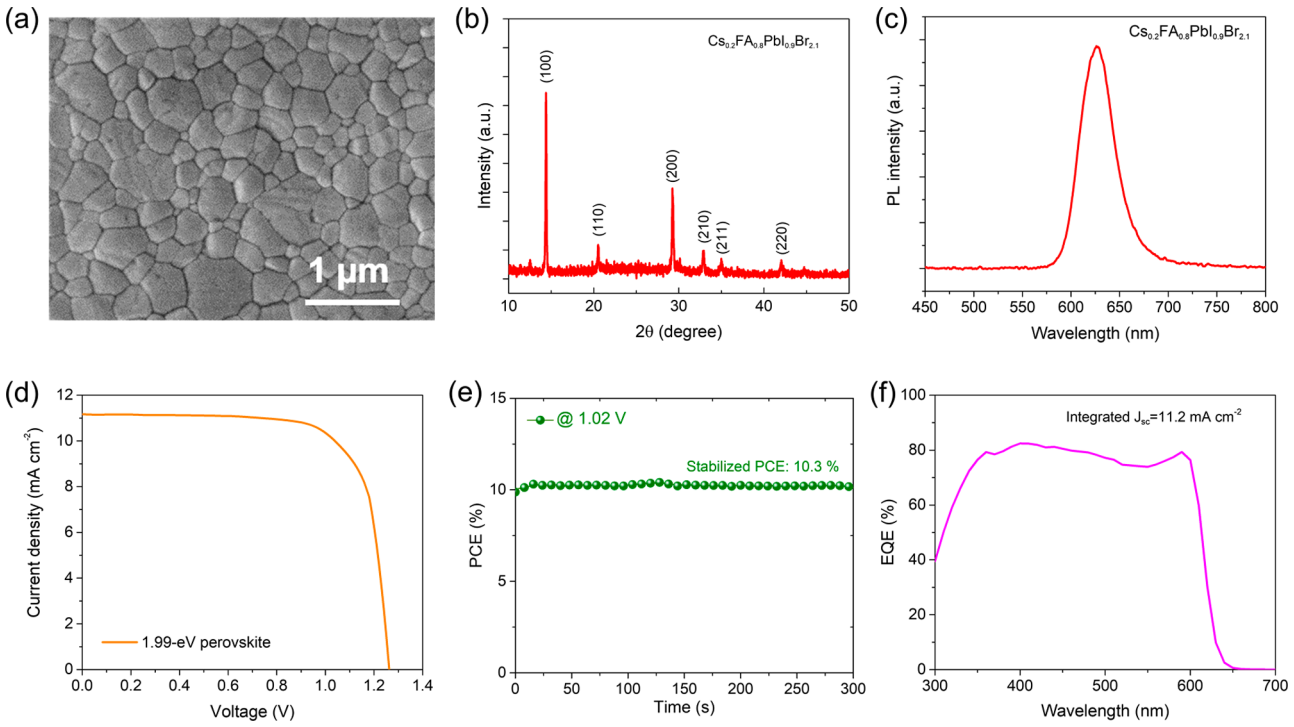

Figure 1. Wide-bandgap (1.99 eV) perovskite with a composition of $Cs_{0.2}FA_{0.8}PbI_{0.9}Br_{2.1}$. (a) Top-view SEM image, (b) XRD pattern, and (c) steady-state PL spectrum of perovskite films. (d) *J*−*V* curve of the champion device. (e) Steady output at the maximum power point. (f) EQE spectrum of the champion device.

solar cells (PSCs) and solvent-tolerant interconnecting layers.[21−25] The highest PCE of 24.8% has been achieved by combining 1.77 and 1.22 eV perovskite subcells and by using dense and robust interconnecting layers with a stack of SnO_2/Au/PEDOT:PSS, where PEDOT:PSS is poly(3,4-ethylenedioxythiophene) polystyrenesulfonate.[26,27] The SnO_2 thin films fabricated by atomic layer deposition (ALD) are compact enough to protect the as-formed front subcell from damage during solution processing of the back subcell.

All-perovskite triple-junction solar cells can feasibly provide even higher efficiency than that available by tandem cells.[28−30] Hörantner et al. evaluated the efficiency of all-perovskite triple-junction devices using material parameters that have been experimentally obtained.[31] This suggests that an all-perovskite triple-junction cell has the potential to raise the feasible efficiency up to ∼37% under ideal light-harvesting conditions using perovskites with bandgaps of 2.04, 1.58, and 1.22 eV, where 1.22 eV is the lowest bandgap value currently achieved for mixed Pb−Sn narrow-bandgap perovskites. It should be noted, however, that perovskites with a lower bandgap (i.e., ∼1.0 eV) should be developed in the future to ensure a significantly higher practical PCE for all-perovskite triple-junction solar cells compared to double-junction devices.[19] A recent material calculation study suggests that a small amount of Cd doping might be able to narrower the bandgap of mixed Pb−Sn perovskites down to ∼1.0 eV.[32]

Despite the high potential efficiency, all-perovskite triple-junction solar cells have rarely been explored experimentally. McMeekin et al. first reported the fabrication of proof-of-concept all-perovskite triple-junction solar cell with a PCE of only 6.7%.[33] It remains challenging to fabricate efficient all-perovskite triple-junction cells because of the following factors. First, it is nontrivial to obtain high-performance subcells with optimal bandgaps. Second, solution processing of a perovskite film often causes damage to the underlying as-formed perovskite layers. Third, it is difficult to obtain thin and conformal charge transport layers (e.g., poly(triaryl amine), PTAA) over surface-rough perovskite subcells by solution processing.[34,35]

Here we report solution-processed all-perovskite triple-junction solar cells with PCEs over 20% via engineering of perovskite bandgaps and interconnecting layers. We developed perovskites with optimal bandgaps of 1.99, 1.60, and 1.22 eV for the front, middle, and back subcells, respectively. We used NiO/PTAA bilayer as the hole transport layer (HTL) for the middle subcell, where the thick NiO layer helps fill the rough surface of the front subcell and thus enables the spin-casting of a thin and more conformal PTAA layer on top. The triple-junction cells achieved a champion PCE of 20.1%, together with a high fill factor (FF) of 81.1% and an open-circuit voltage (V_{oc}) of 2.8 V.

We first aimed to develop a wide-bandgap perovskite having the bandgap of ∼2.0 eV to match the bandgap (1.22 eV) of the back subcell. We fabricated perovskite films with a composition of $Cs_{0.2}FA_{0.8}PbI_{0.9}Br_{2.1}$ using a one-step antisolvent method. $Pb(SCN)_2$ additive (5 mol %) was added into the precursor solution to obtain larger grains (Figures 1a and S1).[36−38] The X-ray diffraction patterns indicate a single cubic perovskite phase with a preferred crystallographic orientation along ⟨100⟩ (Figure 1b). The $Cs_{0.2}FA_{0.8}PbI_{0.9}Br_{2.1}$ perovskite film exhibited a sharp absorption edge and has a Tauc bandgap of 1.99 eV (Figure S2a), consistent with its photoluminescence (PL) peak at 625 nm (Figure 1c).

We then fabricated single-junction solar cells with a p-i-n structure of glass/ITO/PTAA/$Cs_{0.2}FA_{0.8}PbI_{0.9}Br_{2.1}$/$C_{60}$/bathocuproine (BCP)/Cu to evaluate the PV performance. The champion device delivered a V_{oc} of 1.26 V with a short-circuit current density (J_{sc}) of 11.2 mA cm^{-2} and a FF of 73.5%,

https://dx.doi.org/10.1021/acsenergylett.0c01184
ACS Energy Lett. 2020, 5, 2819−2826

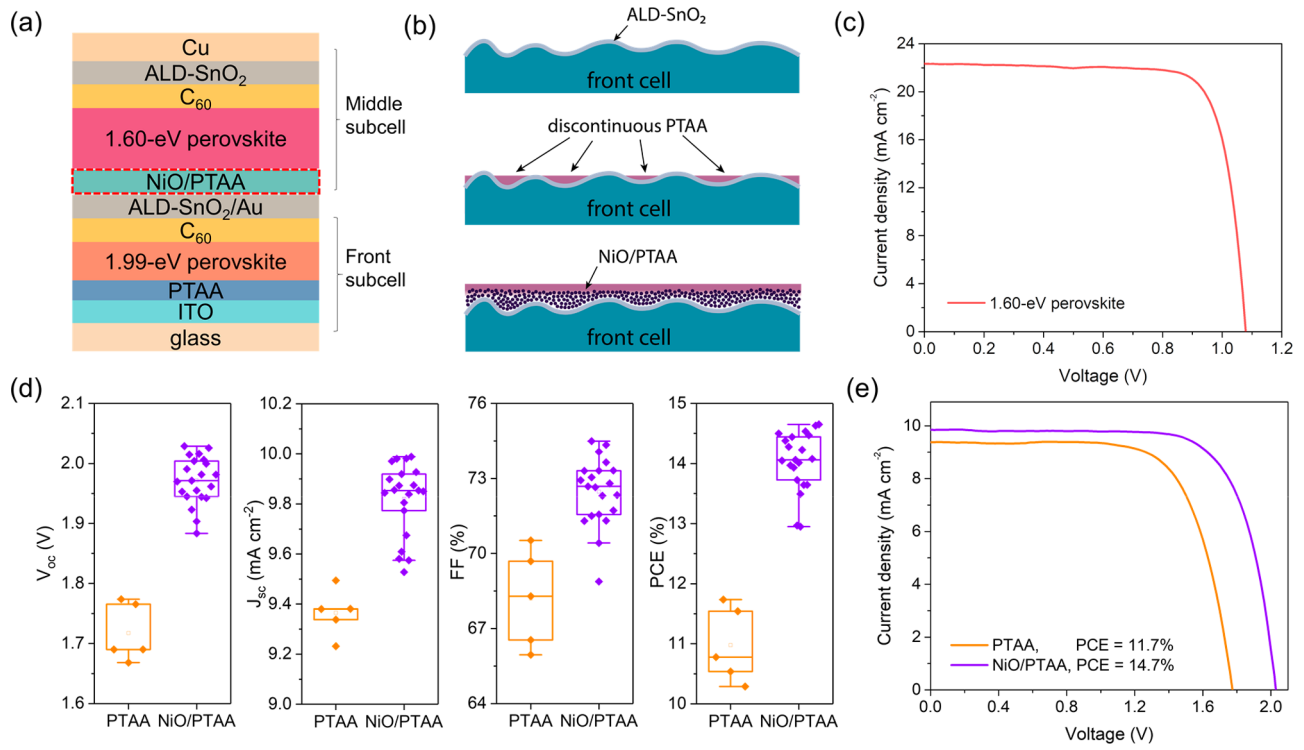

Figure 2. Interconnection between the front (1.99 eV) and middle (1.60 eV) subcells. (a) Device configuration of 1.99 eV/1.60 eV double-junction cell. (b) Schematic diagram of PTAA and NiO/PTAA layers spin-coated on the front subcell. (c) The *J*−*V* curve of a 1.60 eV single-junction perovskite solar cell with NiO/PTAA as the HTL deposited on flat ITO substrate. (d) Statistical PV parameters (V_{oc}, J_{sc}, FF, and PCE) of double-junction cells with PTAA and NiO/PTAA as HTL for the 1.60 eV subcells. (e) *J*−*V* curves of the champion double-junction cells with PTAA and NiO/PTAA for the 1.60 eV subcells.

leading to a PCE of 10.4% under reverse scan (Figure 1d). The corresponding device had a stabilized efficiency of 10.3% under maximum power point tracking over 5 min (Figure 1e). The integrated J_{sc} from external quantum efficiency (EQE) is 11.2 mA cm^{-2}, consistent with the J_{sc} determined from the *J*−*V* characterizations (Figure 1f).

We proceeded to investigate the interconnection between the front and middle subcells as illustrated in Figure 2a. We chose 1.60 eV bandgap perovskite with a composition of $Cs_{0.05}FA_{0.95}PbI_{2.55}Br_{0.45}$ for the middle subcell (Figure S2b). The single-junction cells performed well when fabricated on a flat ITO substrate using PTAA as HTL. However, it became challenging to obtain an efficient middle subcell on top of the surface-rough front subcell when deploying an ultrathin PTAA layer as the HTL (Figure 2d); the necessity of a thin PTAA (i.e., <10 nm) is mainly constrained by its low conductivity.[39] The $Cs_{0.2}FA_{0.8}PbI_{0.9}Br_{2.1}$ perovskite film in the front subcell has a rough surface with vertical peak-to-valley distance >60 nm (Figure S3). The morphology of the 1.99 eV perovskite film was retained after deposition of C_{60} and ALD-SnO_2 layers. When spin-coated directly on the front subcell, the thin PTAA layer could not cover the surface conformally, resulting in a discontinuous HTL layer as illustrated in Figure 2b.

To address this issue, we spin-coated a thick NiO nanocrystal film (~80 nm) prior to the deposition of PTAA. The NiO nanocrystals, with a diameter of ~5 nm, were synthesized according to previous work.[40] The NiO nanocrystals could partially fill the valleys after spin coating and give a less rough surface, which is beneficial to obtain a more compact and pinhole-less PTAA subsequently (Figure 2b). We observed a thicker NiO layer (~80 nm) in the valleys and a thinner layer (~20 nm) on the peaks (Figure S4). We found that the performance of perovskite solar cells was not very sensitive to the thickness of the NiO layer within the range of 20−80 nm, because of its good conductivity (Figure S5). A thin PTAA layer (~8 nm) was further spin-coated on top of the NiO layer because it increases the V_{oc} of the 1.60 eV subcell (Figure S6). The surface root-mean-square roughness of the front subcell obtained from atomic force microscopy (AFM) was reduced from ~26 to ~10 nm after spin coating of NiO/PTAA bilayer (Figure S7). We achieved a similar PCE in 1.60 eV single-junction cells (deposited on flat ITO substrates) using the NiO/PTAA bilayer compared to PTAA single layer (Figures 2c and S6). The use of a thick NiO layer is beneficial to obtain a compact HTL for the subsequent middle subcell, leading to better performance in 1.99 eV/1.60 eV double-junction solar cells (Figure 2d). The double-junction solar cells with bilayer HTL showed considerable improvements in V_{oc} and FF and thus PCE, compared with the devices with PTAA only (Figure 2d,e).

We then fabricated all-perovskite triple-junction solar cells with a device structure as shown in Figure 3a,b. An ultrathin Au cluster layer (ca. 1 nm), fabricated by thermal evaporation, was deployed within the interconnecting layers to facilitate electron−hole recombination between subcells.[26,41] The thickness of the Au layer was optimized to simultaneously have minimal optical absorption loss and sufficient recombination between subcells. The mixed Pb−Sn narrow-bandgap perovskite in the back subcell has a composition of $MA_{0.3}FA_{0.7}Pb_{0.5}Sn_{0.5}I_3$ and a Tauc bandgap of 1.22 eV (Figure S2c). The PEDOT:PSS layer (as HTL for the back subcell) is around 80 nm thick, which is slightly thicker than that used in

https://dx.doi.org/10.1021/acsenergylett.0c01184
ACS Energy Lett. 2020, 5, 2819−2826

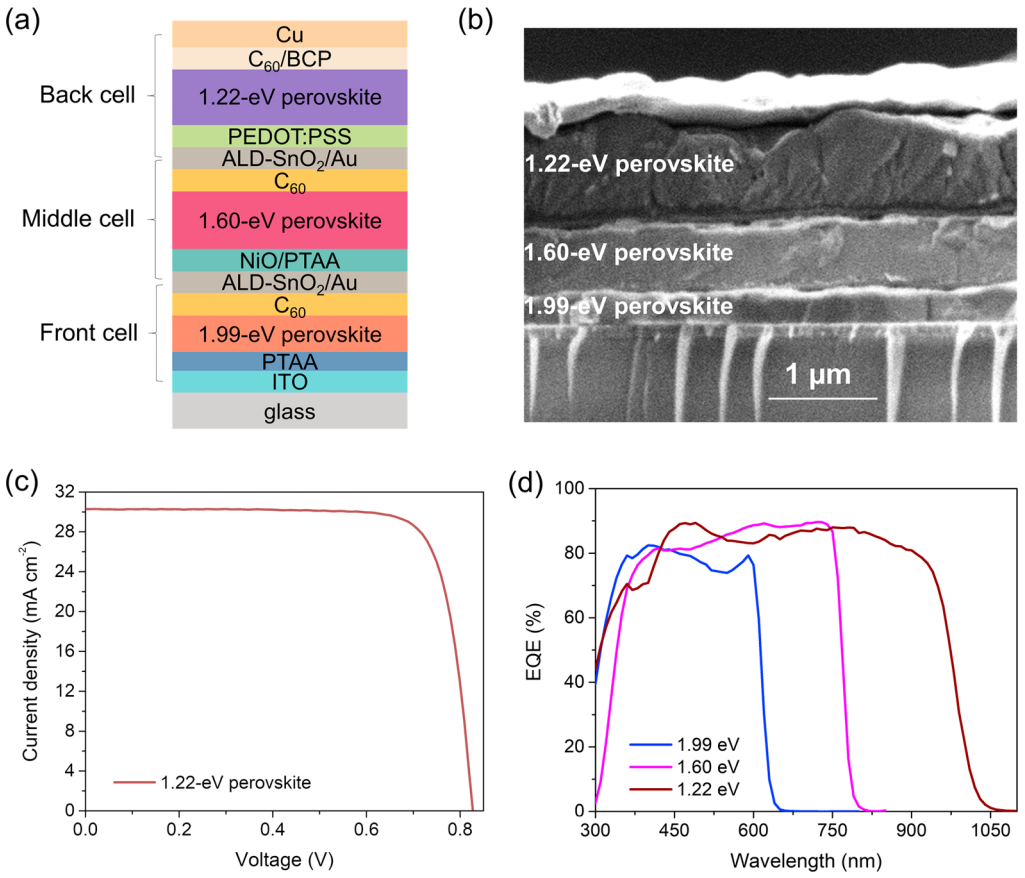

Figure 3. Device structure of all-perovskite triple-junction solar cells. (a) Device configuration and (b) cross-sectional SEM image of all-perovskite triple-junction solar cell. (c) The *J*−*V* curve of a representative 1.22 eV single-junction perovskite solar cell. (d) EQE spectra of the 1.99, 1.60, and 1.22 eV single-junction cells.

single-junction cells to ensure complete coverage on top of the rough middle subcell. Figure 3c presents a typical *J*−*V* curve of a 1.22 eV perovskite solar cell that exhibited a PCE of 20.1% under reverse scan. The PV parameters and EQE spectra of the 1.99, 1.60, and 1.22 eV single-junction cells are summarized in Table 1 and Figure 3d, which clearly show complementary absorption in the wavelength range of 300−1050 nm.

Table 1. Photovoltaic Parameters of Representative Single-Junction Subcells

subcell	V_{oc} (V)	J_{sc} (mA cm^{-2})	FF (%)	PCE (%)
front (1.99 eV)	1.262	11.2	73.5	10.4
middle (1.60 eV)	1.080	22.3	78.8	19.0
back (1.22 eV)	0.828	30.3	80.1	20.1

We first compared the PV performance of triple-junction cells using PTAA and NiO/PTAA in the middle subcells (Table 2 and Figure 4). The statistical PCEs of PTAA and NiO/PTAA devices are presented in Figure 4a. The devices with NiO/PTAA exhibited a significantly higher average PCE than those with PTAA (19.0% vs 15.9%), consistent with the results of double-junction cells discussed above. The best-performing triple-junction cell with PTAA showed a PCE of only 17.2% (V_{oc} = 2.549 V, J_{sc} = 8.9 mA cm^{-2}, and FF = 76.2%). The champion NiO/PTAA device had a significantly improved PCE of 20.1%, together with a V_{oc} of 2.802 V, a J_{sc} of 8.8 mA cm^{-2}, and a FF of 81.1% under reverse scan (Figure 4b and Table 2). The device exhibited a stabilized PCE of 19.8%

Table 2. Photovoltaic Parameters of Champion All-Perovskite Triple-Junction Solar Cells[a]

devices	direction	V_{oc} (V)	J_{sc} (mA cm^{-2})	FF (%)	PCE (%)
double-junction PTAA	reverse	1.774	9.4	70.5	11.7
	forward	1.766	9.4	69.7	11.5
double-junction NiO/PTAA	reverse	2.029	9.9	73.3	14.7
	forward	1.981	9.8	74.3	14.5
triple-junction PTAA	reverse	2.549	8.9	76.2	17.2
	forward	2.543	8.8	76.8	17.2
triple-junction NiO/PTAA	reverse	2.802	8.8	81.1	20.1
	forward	2.793	8.8	80.7	19.9

[a]The performance of 1.99 eV/1.60 eV double junction cells is included as well.

measured over 3 min (Figure 4c) and a minor hysteresis (20.1% vs 19.9%, Figure S8). The integrated J_{sc} values from the corresponding EQE spectra are 8.5, 9.3, and 10.2 mA cm^{-2} for the front, middle, and back subcells, indicating a large current mismatch between subcells (Figure 4d).

We note that the FF achieved in the triple-junction cell herein is higher than those achieved in previous work.[16,33] The relatively high FF is mainly attributed to the large current mismatch between subcells (Figure 4d) and the reduced shunt paths enabled by the thick and compact mixed Pb−Sn subcell, as suggested by the significantly increased shunt resistance (Figure 4b).[42,43] Despite their high FF values, all-perovskite triple-junction cells exhibited a large V_{oc} loss (~370 mV) in

https://dx.doi.org/10.1021/acsenergylett.0c01184
ACS Energy Lett. 2020, 5, 2819−2826

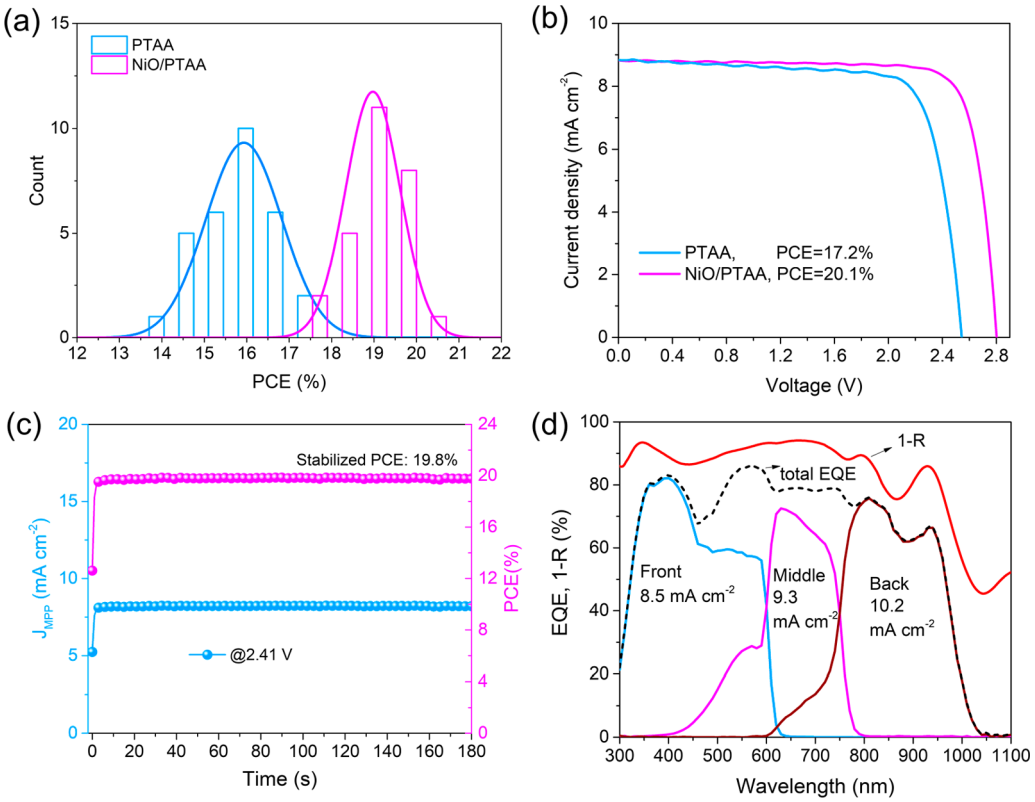

Figure 4. Photovoltaic performance of all-perovskite triple-junction solar cells. (a) PCE distribution of triple-junction cells with PTAA and NiO/PTAA as HTL for the middle subcells. (b) *J*–*V* curves of the champion triple-junction cells with PTAA and NiO/PTAA. (c) Steady-state output of the champion triple-junction cell with NiO/PTAA. (d) EQE and total absorptance (1 − *R*, where *R* is reflectance) spectra of the champion triple-junction cell. The total EQE, sum of the three subcells' EQE, is included as well.

comparison to the summed V_{oc} of three subcells, which can be ascribed to several reasons. The V_{oc} of the front cell was decreased by ∼80 mV after the deposition of ALD-SnO_2 (Figure S9), likely because of the damage from TDMASn and water.[44] The V_{oc} of the front cell was further reduced by ∼30 mV after the spin coating of NiO. Because of the rough surface of the front subcell, it is challenging to obtain a compact and pinhole-free ALD-SnO_2 layer. This might lead to solvent penetration into the front subcell during the following solution processes, causing damage to the front subcell. The nonuniformity of NiO/PTAA on the rough front subcell also led to a severe V_{oc} loss of ∼200 mV in the middle subcell, compared to the devices on flat ITO substrates (see Figure S9 and Table 2). To reduce this V_{oc} loss, conformal coating of HTL on the rough front subcell should be developed in the future, such as sputtered NiO_x or ALD-grown NiO_x, self-assembled monolayer, and evaporated HTL.[45−48] Furthermore, processing of the 1.99 eV wide-bandgap perovskite films remains to be further improved to reduce the surface roughness which will be beneficial to obtain a uniform HTL on top. Several methods have been suggested to form smooth and uniform morphology, such as tuning the precursor solvents, slowing down solvent extraction via blowing gas, and using additives in the precursor solution to slow down crystal growth.[49−51] In general, the middle and back subcells would have slightly lower V_{oc} values (∼30 mV lower for each) than in single-junction cells because of the resistance loss in the interconnecting layers and the reduced light intensity in a multijunction configuration. In addition to avoiding the V_{oc} losses mentioned above, it is crucial in the future to substantially reduce the V_{oc} deficit of each subcell (especially for the 1.99 and 1.60 eV subcells) to achieve a high V_{oc} for triple-junction solar cells.

The relatively low J_{sc} value is another limiting factor for the PCE of all-perovskite triple-junction solar cells. The low J_{sc} is mainly ascribed to the large current mismatch between subcells and high primary optical reflection at the front side (Figure 4d). We further explored the optical modeling of the triple-junction cell by using a validated optical model (GenPro4),[52] together with experimental optical parameter and thickness for each layer. We assume that the current density is limited by the lowest one among the three subcells. The optical simulation suggests that parasitic absorption losses by the front ITO transparent electrode and by the multiple charge transport layers (e.g., C_{60} and PEDOT:PSS layers) also contribute to the optical loss in all-perovskite triple-junction solar cells (Figure S10). The J_{sc} of all-perovskite triple-junction cells can be further increased by optimizing the thickness and bandgap of each absorber to get matched current densities, by reducing the optical reflection losses, by using a front electrode with better transparency in the near-infrared spectral region, and by using more transparent charge transport materials (especially for the HTL in the back subcell).

We carried out preliminary stability tests for all-perovskite triple-junction solar cells. The devices maintained 95% of initial PCE after dark storage in an N_2 glovebox for 325 days (Figure S11a). However, the devices showed a fast performance decay during operation under full AM 1.5G illumination (Figure S11b), mainly because of the photoinduced degradation (e.g., halide segregation) in the 1.99 eV subcell (Figure

https://dx.doi.org/10.1021/acsenergylett.0c01184
ACS Energy Lett. 2020, 5, 2819−2826

S12). Further studies are required to enhance the photostability of wide-bandgap perovskites with a high content of Br.

In summary, we fabricated 20.1%-efficient monolithic all-perovskite triple-junction solar cells by combining perovskites with bandgaps of 1.99, 1.60, and 1.22 eV, where all the perovskite layers were solution processed. A thick bilayered NiO/PTAA was developed and deployed for the HTL in the middle subcell. Compared to PTAA single layer, the bilayered HTL can achieve a better surface coverage on top of the rough front subcell, leading to significantly improved V_{oc} and FF. Nevertheless, there remain challenges that need to be addressed to leverage the full potential of all-perovskite triple-junction solar cells. Overall, we here demonstrate that high-performance all-perovskite triple-junction solar cells can be fabricated with commonly used solution-processing techniques. Given the explosion of interest and rapid progress in all-perovskite multijunction solar cells, we anticipate that PCEs beyond 30% could be achieved in the near future.

■ ASSOCIATED CONTENT

Supporting Information

The Supporting Information is available free of charge at https://pubs.acs.org/doi/10.1021/acsenergylett.0c01184.

Experimental methods for triple-junction solar cell fabrication; details on the device characterization; additional top-view and cross-sectional SEM images; AFM images; Tauc plot fitting; optical simulation data (PDF)

■ AUTHOR INFORMATION

Corresponding Author

Hairen Tan − *National Laboratory of Solid State Microstructures, Jiangsu Key Laboratory of Artificial Functional Materials, College of Engineering and Applied Sciences, Nanjing University, Nanjing 210093, China;* orcid.org/0000-0003-0821-476X; Email: hairentan@nju.edu.cn

Authors

Ke Xiao − *National Laboratory of Solid State Microstructures, Jiangsu Key Laboratory of Artificial Functional Materials, College of Engineering and Applied Sciences and School of Electronics Science and Engineering, Nanjing University, Nanjing 210093, China*

Jin Wen − *National Laboratory of Solid State Microstructures, Jiangsu Key Laboratory of Artificial Functional Materials, College of Engineering and Applied Sciences, Nanjing University, Nanjing 210093, China*

Qiaolei Han − *National Laboratory of Solid State Microstructures, Jiangsu Key Laboratory of Artificial Functional Materials, College of Engineering and Applied Sciences, Nanjing University, Nanjing 210093, China*

Renxing Lin − *National Laboratory of Solid State Microstructures, Jiangsu Key Laboratory of Artificial Functional Materials, College of Engineering and Applied Sciences, Nanjing University, Nanjing 210093, China*

Yuan Gao − *National Laboratory of Solid State Microstructures, Jiangsu Key Laboratory of Artificial Functional Materials, College of Engineering and Applied Sciences, Nanjing University, Nanjing 210093, China*

Shuai Gu − *National Laboratory of Solid State Microstructures, Jiangsu Key Laboratory of Artificial Functional Materials, College of Engineering and Applied Sciences, Nanjing University, Nanjing 210093, China*

Yipeng Zang − *National Laboratory of Solid State Microstructures, Jiangsu Key Laboratory of Artificial Functional Materials, College of Engineering and Applied Sciences, Nanjing University, Nanjing 210093, China*

Yuefeng Nie − *National Laboratory of Solid State Microstructures, Jiangsu Key Laboratory of Artificial Functional Materials, College of Engineering and Applied Sciences, Nanjing University, Nanjing 210093, China*

Jia Zhu − *National Laboratory of Solid State Microstructures, Jiangsu Key Laboratory of Artificial Functional Materials, College of Engineering and Applied Sciences, Nanjing University, Nanjing 210093, China;* orcid.org/0000-0002-2871-4369

Jun Xu − *School of Electronics Science and Engineering, Nanjing University, Nanjing 210093, China;* orcid.org/0000-0002-0469-9766

Complete contact information is available at: https://pubs.acs.org/10.1021/acsenergylett.0c01184

Author Contributions

[§]K.X. and J.W. contributed equally to this work.

Notes

The authors declare no competing financial interest.

■ ACKNOWLEDGMENTS

This work was financially supported by the National Natural Science Foundation of China (61974063), the National Key R&D Program of China (2018YFB1500102), Natural Science Foundation of Jiangsu Province (BK20190315), the Fundamental Research Funds for the Central Universities (14380168), the Thousand Talent Program for Young Outstanding Scientists in China, and Program for Innovative Talents and Entrepreneur in Jiangsu.

■ REFERENCES

(1) ITRPV. *International Technology Roadmap for Photovoltaic - 2016 Results*; 2017.

(2) Yoshikawa, K.; Kawasaki, H.; Yoshida, W.; Irie, T.; Konishi, K.; Nakano, K.; Uto, T.; Adachi, D.; Kanematsu, M.; Uzu, H.; Yamamoto, K. Silicon Heterojunction Solar Cell with Interdigitated Back Contacts for a Photoconversion Efficiency over 26%. *Nat. Energy* **2017**, *2*, 17032.

(3) Martí, A.; Araújo, G. L. Limiting Efficiencies for Photovoltaic Energy Conversion in Multigap Systems. *Sol. Energy Mater. Sol. Cells* **1996**, *43* (2), 203−222.

(4) McMahon, W. E.; Friedman, D. J.; Geisz, J. F. Multijunction Solar Cell Design Revisited: Disruption of Current Matching by Atmospheric Absorption Bands. *Prog. Photovoltaics* **2017**, *25* (10), 850−860.

(5) Henry, C. H. Limiting Efficiencies of Ideal Single and Multiple Energy Gap Terrestrial Solar Cells. *J. Appl. Phys.* **1980**, *51* (8), 4494−4500.

(6) Green, M. A.; Dunlop, E. D.; Hohl-Ebinger, J.; Yoshita, M.; Kopidakis, N.; Ho-Baillie, A. W. Y. Solar Cell Efficiency Tables (Version 55). *Prog. Photovoltaics* **2020**, *28* (1), 3−15.

(7) Geisz, J. F.; France, R. M.; Schulte, K. L.; Steiner, M. A.; Norman, A. G.; Guthrey, H. L.; Young, M. R.; Song, T.; Moriarty, T. Six-Junction III−V Solar Cells with 47.1% Conversion Efficiency under 143 Suns Concentration. *Nat. Energy* **2020**, *5* (4), 326−335.

(8) Greenaway, A. L.; Boucher, J. W.; Oener, S. Z.; Funch, C. J.; Boettcher, S. W. Low-Cost Approaches to III−V Semiconductor Growth for Photovoltaic Applications. *ACS Energy Lett.* **2017**, *2* (10), 2270−2282.

(9) Bobela, D. C.; Gedvilas, L.; Woodhouse, M.; Horowitz, K. A. W.; Basore, P. A. Economic Competitiveness of III-V on Silicon Tandem One-Sun Photovoltaic Solar Modules in Favorable Future Scenarios. *Prog. Photovoltaics* **2017**, *25* (1), 41−48.
(10) Bosi, M.; Pelosi, C. The Potential of III-V Semiconductors as Terrestrial Photovoltaic Devices. *Prog. Photovoltaics* **2007**, *15* (1), 51−68.
(11) Chen, Q.; De Marco, N.; Yang, Y.; Song, T.-B.; Chen, C.-C.; Zhao, H.; Hong, Z.; Zhou, H.; Yang, Y. Under the Spotlight: The Organic−Inorganic Hybrid Halide Perovskite for Optoelectronic Applications. *Nano Today* **2015**, *10* (3), 355−396.
(12) Tan, H.; Che, F.; Wei, M.; Zhao, Y.; Saidaminov, M. I.; Todorović, P.; Broberg, D.; Walters, G.; Tan, F.; Zhuang, T.; Sun, B.; Liang, Z.; Yuan, H.; Fron, E.; Kim, J.; Yang, Z.; Voznyy, O.; Asta, M.; Sargent, E. H. Dipolar Cations Confer Defect Tolerance in Wide-Bandgap Metal Halide Perovskites. *Nat. Commun.* **2018**, *9* (1), 3100.
(13) Jeon, N. J.; Noh, J. H.; Kim, Y. C.; Yang, W. S.; Ryu, S.; Seok, S. Il. Solvent Engineering for High-Performance Inorganic−Organic Hybrid Perovskite Solar Cells. *Nat. Mater.* **2014**, *13* (9), 897−903.
(14) Tao, S.; Schmidt, I.; Brocks, G.; Jiang, J.; Tranca, I.; Meerholz, K.; Olthof, S. Absolute Energy Level Positions in Tin- and Lead-Based Halide Perovskites. *Nat. Commun.* **2019**, *10* (1), 2560.
(15) NREL. Best Research-Cell Efficiencies. https://www.nrel.gov/pv/assets/pdfs/best-research-cell-efficiencies.20200218.pdf.
(16) Werner, J.; Sahli, F.; Fu, F.; Diaz Leon, J. J.; Walter, A.; Kamino, B. A.; Niesen, B.; Nicolay, S.; Jeangros, Q.; Ballif, C. Perovskite/Perovskite/Silicon Monolithic Triple-Junction Solar Cells with a Fully Textured Design. *ACS Energy Lett.* **2018**, *3* (9), 2052−2058.
(17) Noh, J. H.; Im, S. H.; Heo, J. H.; Mandal, T. N.; Seok, S. Il. Chemical Management for Colorful, Efficient, and Stable Inorganic-Organic Hybrid Nanostructured Solar Cells. *Nano Lett.* **2013**, *13* (4), 1764−1769.
(18) Hao, F.; Stoumpos, C. C.; Chang, R. P. H.; Kanatzidis, M. G. Anomalous Band Gap Behavior in Mixed Sn and Pb Perovskites Enables Broadening of Absorption Spectrum in Solar Cells. *J. Am. Chem. Soc.* **2014**, *136* (22), 8094−8099.
(19) Eperon, G. E.; Hörantner, M. T.; Snaith, H. J. Metal Halide Perovskite Tandem and Multiple-Junction Photovoltaics. *Nat. Rev. Chem.* **2017**, *1*, 95.
(20) Leijtens, T.; Bush, K. A.; Prasanna, R.; McGehee, M. D. Opportunities and Challenges for Tandem Solar Cells Using Metal Halide Perovskite Semiconductors. *Nat. Energy* **2018**, *3* (10), 828−838.
(21) Wang, Y.; Zhang, M.; Xiao, K.; Lin, R.; Luo, X.; Han, Q.; Tan, H. Recent Progress in Developing Efficient Monolithic All-Perovskite Tandem Solar Cells. *J. Semicond.* **2020**, *41* (5), 051201.
(22) Gu, S.; Lin, R.; Han, Q.; Gao, Y.; Tan, H.; Zhu, J. Tin and Mixed Lead−Tin Halide Perovskite Solar Cells: Progress and Their Application in Tandem Solar Cells. *Adv. Mater.* **2020**, 1907392.
(23) Yang, Z.; Yu, Z.; Wei, H.; Xiao, X.; Ni, Z.; Chen, B.; Deng, Y.; Habisreutinger, S. N.; Chen, X.; Wang, K.; Zhao, J.; Rudd, P. N.; Berry, J. J.; Beard, M. C.; Huang, J. Enhancing Electron Diffusion Length in Narrow-Bandgap Perovskites for Efficient Monolithic Perovskite Tandem Solar Cells. *Nat. Commun.* **2019**, *10* (1), 4498.
(24) Tong, J.; Song, Z.; Kim, D. H.; Chen, X.; Chen, C.; Palmstrom, A. F.; Ndione, P. F.; Reese, M. O.; Dunfield, S. P.; Reid, O. G.; Liu, J.; Zhang, F.; Harvey, S. P.; Li, Z.; Christensen, S. T.; Teeter, G.; Zhao, D.; Al-Jassim, M. M.; Van Hest, M. F. A. M.; Beard, M. C.; Shaheen, S. E.; Berry, J. J.; Yan, Y.; Zhu, K. Carrier Lifetimes of > 1 Ms in Sn-Pb Perovskites Enable Efficient All-Perovskite Tandem Solar Cells. *Science* **2019**, *364* (6439), 475−479.
(25) Zhao, D.; Chen, C.; Wang, C.; Junda, M. M.; Song, Z.; Grice, C. R.; Yu, Y.; Li, C.; Subedi, B.; Podraza, N. J.; Zhao, X.; Fang, G.; Xiong, R. G.; Zhu, K.; Yan, Y. Efficient Two-Terminal All-Perovskite Tandem Solar Cells Enabled by High-Quality Low-Bandgap Absorber Layers. *Nat. Energy* **2018**, *3* (12), 1093−1100.
(26) Lin, R.; Xiao, K.; Qin, Z.; Han, Q.; Zhang, C.; Wei, M.; Saidaminov, M. I.; Gao, Y.; Xu, J.; Xiao, M.; Li, A.; Zhu, J.; Sargent, E. H.; Tan, H. Monolithic All-Perovskite Tandem Solar Cells with 24.8% Efficiency Exploiting Comproportionation to Suppress Sn(Ii) Oxidation in Precursor Ink. *Nat. Energy* **2019**, *4* (10), 864−873.
(27) Wei, M.; Xiao, K.; Walters, G.; Lin, R.; Zhao, Y.; Saidaminov, M. I.; Todorović, P.; Johnston, A.; Huang, Z.; Chen, H.; Li, A.; Zhu, J.; Yang, Z.; Wang, Y.; Proppe, A. H.; Kelley, S. O.; Hou, Y.; Voznyy, O.; Tan, H.; Sargent, E. H. Combining Efficiency and Stability in Mixed Tin−Lead Perovskite Solar Cells by Capping Grains with an Ultrathin 2D Layer. *Adv. Mater.* **2020**, *32* (12), 1907058.
(28) Cariou, R.; Benick, J.; Feldmann, F.; Höhn, O.; Hauser, H.; Beutel, P.; Razek, N.; Wimplinger, M.; Bläsi, B.; Lackner, D.; Hermle, M.; Siefer, G.; Glunz, S. W.; Bett, A. W.; Dimroth, F. III−V-on-Silicon Solar Cells Reaching 33% Photoconversion Efficiency in Two-Terminal Configuration. *Nat. Energy* **2018**, *3* (4), 326−333.
(29) Schüttauf, J.-W.; Niesen, B.; Löfgren, L.; Bonnet-Eymard, M.; Stuckelberger, M.; Hänni, S.; Boccard, M.; Bugnon, G.; Despeisse, M.; Haug, F.-J.; Meillaud, F.; Ballif, C. Amorphous Silicon−Germanium for Triple and Quadruple Junction Thin-Film Silicon Based Solar Cells. *Sol. Energy Mater. Sol. Cells* **2015**, *133*, 163−169.
(30) Essig, S.; Allebé, C.; Remo, T.; Geisz, J. F.; Steiner, M. A.; Horowitz, K.; Barraud, L.; Ward, J. S.; Schnabel, M.; Descoeudres, A.; Young, D. L.; Woodhouse, M.; Despeisse, M.; Ballif, C.; Tamboli, A. Raising the One-Sun Conversion Efficiency of III−V/Si Solar Cells to 32.8% for Two Junctions and 35.9% for Three Junctions. *Nat. Energy* **2017**, *2*, 17144.
(31) Hörantner, M. T.; Leijtens, T.; Ziffer, M. E.; Eperon, G. E.; Christoforo, M. G.; McGehee, M. D.; Snaith, H. J. The Potential of Multijunction Perovskite Solar Cells. *ACS Energy Lett.* **2017**, *2* (10), 2506−2513.
(32) Choubisa, H.; Askerka, M.; Ryczko, K.; Voznyy, O.; Mills, K.; Tamblyn, I.; Sargent, E. H. Crystal Site Feature Embedding Enables Exploration of Large Chemical Spaces. *Matter* **2020**, *3*, 433.
(33) McMeekin, D. P.; Mahesh, S.; Noel, N. K.; Klug, M. T.; Lim, J. C.; Warby, J. H.; Ball, J. M.; Herz, L. M.; Johnston, M. B.; Snaith, H. J. Solution-Processed All-Perovskite Multi-Junction Solar Cells. *Joule* **2019**, *3* (2), 387−401.
(34) Li, C.; Pan, Y.; Hu, J.; Qiu, S.; Zhang, C.; Yang, Y.; Chen, S.; Liu, X.; Brabec, C. J.; Nazeeruddin, M. K.; Mai, Y.; Guo, F. Vertically Aligned 2D/3D Pb-Sn Perovskites with Enhanced Charge Extraction and Suppressed Phase Segregation for Efficient Printable Solar Cells. *ACS Energy Lett.* **2020**, *5*, 1386−1395.
(35) Stolterfoht, M.; Wolff, C. M.; Márquez, J. A.; Zhang, S.; Hages, C. J.; Rothhardt, D.; Albrecht, S.; Burn, P. L.; Meredith, P.; Unold, T.; Neher, D. Visualization and Suppression of Interfacial Recombination for High-Efficiency Large-Area Pin Perovskite Solar Cells. *Nat. Energy* **2018**, *3* (10), 847−854.
(36) Kim, D. H.; Muzzillo, C. P.; Tong, J.; Palmstrom, A. F.; Larson, B. W.; Choi, C.; Harvey, S. P.; Glynn, S.; Whitaker, J. B.; Zhang, F.; Li, Z.; Lu, H.; van Hest, M. F. A. M.; Berry, J. J.; Mansfield, L. M.; Huang, Y.; Yan, Y.; Zhu, K. Bimolecular Additives Improve Wide-Band-Gap Perovskites for Efficient Tandem Solar Cells with CIGS. *Joule* **2019**, *3* (7), 1734−1745.
(37) Zhou, Y.; Jia, Y. H.; Fang, H. H.; Loi, M. A.; Xie, F. Y.; Gong, L.; Qin, M. C.; Lu, X. H.; Wong, C. P.; Zhao, N. Composition-Tuned Wide Bandgap Perovskites: From Grain Engineering to Stability and Performance Improvement. *Adv. Funct. Mater.* **2018**, *28* (35), 1803130.
(38) Yu, Y.; Wang, C.; Grice, C. R.; Shrestha, N.; Zhao, D.; Liao, W.; Guan, L.; Awni, R. A.; Meng, W.; Cimaroli, A. J.; Zhu, K.; Ellingson, R. J.; Yan, Y. Synergistic Effects of Lead Thiocyanate Additive and Solvent Annealing on the Performance of Wide-Bandgap Perovskite Solar Cells. *ACS Energy Lett.* **2017**, *2* (5), 1177−1182.
(39) Stolterfoht, M.; Wolff, C. M.; Amir, Y.; Paulke, A.; Perdigón-Toro, L.; Caprioglio, P.; Neher, D. Approaching the Fill Factor Shockley-Queisser Limit in Stable, Dopant-Free Triple Cation Perovskite Solar Cells. *Energy Environ. Sci.* **2017**, *10* (6), 1530−1539.
(40) Han, Q.; Wei, Y.; Lin, R.; Fang, Z.; Xiao, K.; Luo, X.; Gu, S.; Zhu, J.; Ding, L.; Tan, H. Low-Temperature Processed Inorganic

Hole Transport Layer for Efficient and Stable Mixed Pb-Sn Low-Bandgap Perovskite Solar Cells. *Sci. Bull.* **2019**, *64* (19), 1399−1401.
(41) Kim, T.; Firdaus, Y.; Kirmani, A. R.; Liang, R. Z.; Hu, H.; Liu, M.; El Labban, A.; Hoogland, S.; Beaujuge, P. M.; Sargent, E. H.; Amassian, A. Hybrid Tandem Quantum Dot/Organic Solar Cells with Enhanced Photocurrent and Efficiency via Ink and Interlayer Engineering. *ACS Energy Lett.* **2018**, *3* (6), 1307−1314.
(42) Köhnen, E.; Jošt, M.; Morales-Vilches, A. B.; Tockhorn, P.; Al-Ashouri, A.; Macco, B.; Kegelmann, L.; Korte, L.; Rech, B.; Schlatmann, R.; Stannowski, B.; Albrecht, S. Highly Efficient Monolithic Perovskite Silicon Tandem Solar Cells: Analyzing the Influence of Current Mismatch on Device Performance. *Sustain. Energy Fuels* **2019**, *3* (8), 1995−2005.
(43) Boccard, M.; Ballif, C. Influence of the Subcell Properties on the Fill Factor of Two-Terminal Perovskite-Silicon Tandem Solar Cells. *ACS Energy Lett.* **2020**, *5* (4), 1077−1082.
(44) Palmstrom, A. F.; Raiford, J. A.; Prasanna, R.; Bush, K. A.; Sponseller, M.; Cheacharoen, R.; Minichetti, M. C.; Bergsman, D. S.; Leijtens, T.; Wang, H.-P.; Bulović, V.; McGehee, M. D.; Bent, S. F. Interfacial Effects of Tin Oxide Atomic Layer Deposition in Metal Halide Perovskite Photovoltaics. *Adv. Energy Mater.* **2018**, *8* (23), 1800591.
(45) Hou, Y.; Aydin, E.; De Bastiani, M.; Xiao, C.; Isikgor, F. H.; Xue, D. J.; Chen, B.; Chen, H.; Bahrami, B.; Chowdhury, A. H.; Johnston, A.; Baek, S. W.; Huang, Z.; Wei, M.; Dong, Y.; Troughton, J.; Jalmood, R.; Mirabelli, A. J.; Allen, T. G.; Van Kerschaver, E.; Saidaminov, M. I.; Baran, D.; Qiao, Q.; Zhu, K.; De Wolf, S.; Sargent, E. H. Efficient Tandem Solar Cells with Solution-Processed Perovskite on Textured Crystalline Silicon. *Science* **2020**, *367* (6482), 1135−1140.
(46) Jošt, M.; Bertram, T.; Koushik, D.; Marquez, J. A.; Verheijen, M. A.; Heinemann, M. D.; Köhnen, E.; Al-Ashouri, A.; Braunger, S.; Lang, F.; Rech, B.; Unold, T.; Creatore, M.; Lauermann, I.; Kaufmann, C. A.; Schlatmann, R.; Albrecht, S. 21.6%-Efficient Monolithic Perovskite/Cu(In,Ga)Se 2 Tandem Solar Cells with Thin Conformal Hole Transport Layers for Integration on Rough Bottom Cell Surfaces. *ACS Energy Lett.* **2019**, *4* (2), 583−590.
(47) Al-Ashouri, A.; Magomedov, A.; Roß, M.; Jošt, M.; Talaikis, M.; Chistiakova, G.; Bertram, T.; Márquez, J. A.; Köhnen, E.; Kasparavičius, E.; Levcenco, S.; Gil-Escrig, L.; Hages, C. J.; Schlatmann, R.; Rech, B.; Malinauskas, T.; Unold, T.; Kaufmann, C. A.; Korte, L.; Niaura, G.; Getautis, V.; Albrecht, S. Conformal Monolayer Contacts with Lossless Interfaces for Perovskite Single Junction and Monolithic Tandem Solar Cells. *Energy Environ. Sci.* **2019**, *12* (11), 3356−3369.
(48) Sahli, F.; Werner, J.; Kamino, B. A.; Bräuninger, M.; Monnard, R.; Paviet-Salomon, B.; Barraud, L.; Ding, L.; Diaz Leon, J. J.; Sacchetto, D.; Cattaneo, G.; Despeisse, M.; Boccard, M.; Nicolay, S.; Jeangros, Q.; Niesen, B.; Ballif, C. Fully Textured Monolithic Perovskite/Silicon Tandem Solar Cells with 25.2% Power Conversion Efficiency. *Nat. Mater.* **2018**, *17* (9), 820−826.
(49) Bush, K. A.; Rolston, N.; Gold-Parker, A.; Manzoor, S.; Hausele, J.; Yu, Z. J.; Raiford, J. A.; Cheacharoen, R.; Holman, Z. C.; Toney, M. F.; Dauskardt, R. H.; McGehee, M. D. Controlling Thin-Film Stress and Wrinkling during Perovskite Film Formation. *ACS Energy Lett.* **2018**, *3* (6), 1225−1232.
(50) Werner, J.; Moot, T.; Gossett, T. A.; Gould, I. E.; Palmstrom, A. F.; Wolf, E. J.; Boyd, C. C.; Van Hest, M. F. A. M.; Luther, J. M.; Berry, J. J.; McGehee, M. D. Improving Low-Bandgap Tin-Lead Perovskite Solar Cells via Contact Engineering and Gas Quench Processing. *ACS Energy Lett.* **2020**, *5* (4), 1215−1223.
(51) Li, Z.; Kim, T. H.; Han, S. Y.; Yun, Y. J.; Jeong, S.; Jo, B.; Ok, S. A.; Yim, W.; Lee, S. H.; Kim, K.; Moon, S.; Park, J. Y.; Ahn, T. K.; Shin, H.; Lee, J.; Park, H. J. Wide-Bandgap Perovskite/Gallium Arsenide Tandem Solar Cells. *Adv. Energy Mater.* **2020**, *10* (6), 1903085.
(52) Santbergen, R.; Meguro, T.; Suezaki, T.; Koizumi, G.; Yamamoto, K.; Zeman, M. GenPro4 Optical Model for Solar Cell Simulation and Its Application to Multijunction Solar Cells. *IEEE J. Photovoltaics* **2017**, *7* (3), 919−926.

https://dx.doi.org/10.1021/acsenergylett.0c01184
ACS Energy Lett. 2020, 5, 2819−2826